Development of High Gain GaN/AlGaN Avalanche Photodiode Arrays for UV Detection and Imaging Applications

Ashok K. Sood, John W. Zeller and Yash R. Puri
Magnolia Optical Technologies Inc., 52-B Cummings Park, Woburn, MA 01801

Russell D. Dupuis, Theeradetch Detchprohm, Mi-Hee Ji, and Shyh-Chiang Shen
School of Electrical Engineering, Georgia Institute of Technology, Atlanta, GA 30332

Sachidananda Babu
NASA Earth Science Technology Office, Goddard Space Flight Center, Greenbelt, MD 20771

Nibir K. Dhar
U.S. Army Night Vision and Electronic Sensors Directorate, Fort Belvoir, VA 22060

Priyalal Wijewarnasuriya
U.S. Army Research Laboratory, 2800 Powder Mill Road, Adelphi, MD 20783

ABSTRACT

Sensing and imaging over ultraviolet (UV) bands has many applications for defense and commercial systems, as shorter wavelengths allow for increased spatial resolution, smaller pixels, and larger formats. The next frontier is to develop UV avalanche photodiode (UV-APD) arrays with high gain to demonstrate high-resolution imaging. Various GaN/AlGaN *p-i-n* UV-APDs have been fabricated from epitaxial structures grown by metalorganic chemical vapor deposition (MOCVD) on low dislocation density substrates. The performance characteristics of frontside-illuminated UV-APDs grown on GaN/sapphire templates were compared with UV-APDs grown on free-standing (FS) GaN substrates, where the latter demonstrated lower dark

current densities for all fabricated mesa sizes, stable avalanche gains higher than 5×10^5, and significantly higher responsivities. In addition, UV-APD epitaxial structures were fabricated in 4×4 arrays with large detector areas, showing uniform and reliable distribution of breakdown voltage and leakage current densities. The high crystalline quality of the epitaxial layers of the GaN and $Al_{0.05}Ga_{0.95}N$ UV-APDs combined with the low dislocation densities of the GaN substrates are believed to be responsible for the low leakage currents, enhanced sensitivities, and reliability of the UV-APD devices. This paper will discuss the growth and fabrication, characterization, and performance results of small unit cell size and high gain APDs in wide-bandgap semiconductors, for UV imaging applications.

1. INTRODUCTION

Detection and identification of targets at various distances has traditionally been achieved using a wide range of wavelengths and imaging technologies, which include image intensifies and photomultiplier tubes for UV detection, visible cameras predominately based on silicon technologies, and infrared sensing technologies such as short-wave infrared (SWIR), mid-wave infrared (MWIR), and long-wave infrared (LWIR) imagers [1]. Each have distinct advantages and drawbacks, with their practical utility in a given situation or application largely dependent on the specific set of operating conditions such as light intensity, thermal conditions, and degree of atmospheric obscuration [2]. Using the shortest wavelength practical, i.e., in the UV or visible, is often desired to maximize spatial resolution, which allows for small pixels and large formats [3-6]. Since the longer UV wavelengths transmit through the atmosphere fairly well, and UV radiation is relatively covert in that it is not discernable by the human eye, UV illumination is often preferred over visible. For many applications, the UV band known as the solar-blind region, which is generally considered as comprising deep ultraviolet (DUV) wavelengths of 280 nm and shorter, is optimal. Over this range, virtually all solar radiation is absorbed by the upper atmospheric ozone layer, leaving a dark and clutter-free background even in bright daylight that can greatly facilitate the detection of potential targets.

UV detection has traditionally been dominated by photomultiplier tube (PMT) and silicon-based technologies. PMTs can provide enhanced sensitivity for UV detection with internal gains as high as 10^6 [7]. However, they require very high operating voltages (above 1,200 V) as well photocathode cooling for low-noise performance, making their implementation relatively expensive, bulky, and fragile [8]. In addition, both PMTs and silicon-based detectors require extra filtering in order to be used for operation in the solar-blind spectral region [9].

In recent years, avalanche photodiodes (APDs) based on $Al_xGa_{1-x}N$ semiconductor alloys have attracted significant interest for the detection of photons in the DUV spectral region [10,11]. III-N materials can provide intrinsic detection capability through adjusting the bandgap energy, as well as chemical and thermal stability [8]. In addition, UV-APDs based on GaN/AlGaN can provide advantages of high optical gain, high sensitivity, and low dark current compared to other UV detection technologies [12,13]. Furthermore, the development of focal plane arrays (FPAs) comprising individual APD elements as pixels as small as 4 microns is achievable with this material system technology to provide solar-blind UV imaging capability [2]. Based on these properties and features, AlGaN-based UV-APDs are excellent candidates to replace PMTs for detection of solar-blind radiation in many demanding applications.
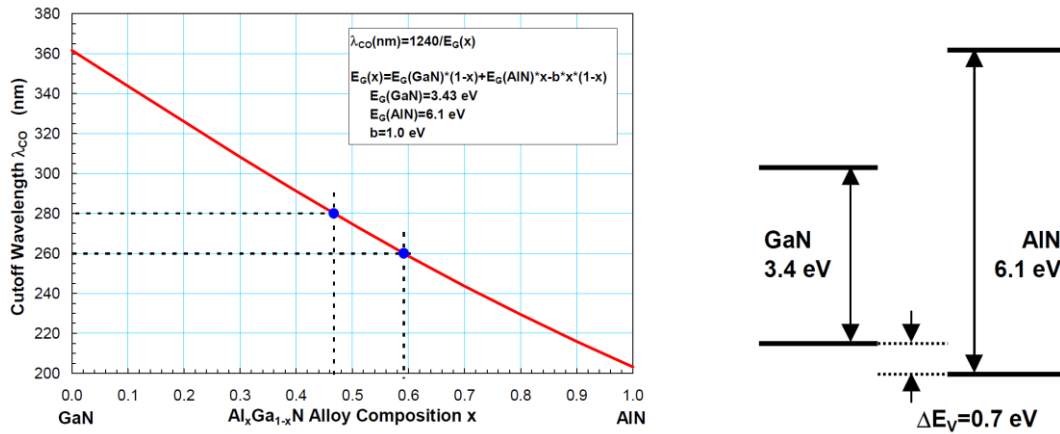

Figure 1. Relationship between alloy composition of AlGaN and the corresponding spectral cutoff wavelength for UV detectors [4].

Figure 1 presents the relationship between the alloy composition of gallium and aluminum in $Al_xGa_{1-x}N$ that determines the cutoff wavelength for *p-i-n* UV detectors, and likewise for UV-APDs comprising absorber layers composed of such material [4]. It is seen that to move towards shorter-wavelength DUV detection capability, including operation over the solar-blind region, incorporation of greater aluminum composition in $Al_xGa_{1-x}N$ is required. While there are several difficulties involved with adding high concentrations of Al in $Al_xGa_{1-x}N$ that impact the crystalline quality of AlGaN, efforts are ongoing to improve the material quality in this regard.

Employing optimum growth parameters on low dislocation density bulk substrates has been successfully employed to improve the crystalline and structural quality of

epitaxial layers by minimizing defect density in epitaxially grown materials. GaN/AlGaN *p-i-n* UV-APD arrays are well-suited for numerous applications including covert military sensing, chemical and biological detection of surface residues and bio-aerosol agents, machine vision, and space research [14]. The next frontier is to develop and demonstrate high performance, small unit cell / pixel size GaN/AlGaN UV-APD arrays for sensors to enable high resolution imaging in UV bands of interest, including the solar-blind region.

Due to the lack of availability of native III-N substrates, the development of large-area UV-APD arrays based on III-N materials has been primarily limited to the use of lattice-mismatched substrates such as SiC and sapphire [15]. However, the lattice mismatch and difference in the thermal expansion coefficients between such foreign substrates and the deposited epitaxial layers leads to cracking and/or bowing of material structures and other strain-induced defects, in particular threading dislocations, resulting in high leakage current and premature microplasma breakdown prior to reaching avalanche breakdown [16,17]. This has in turn resulted in UV-APD devices having nonuniform electrical properties, low yield, and relatively high leakage currents. Consequently, improving the crystalline quality of epitaxial layer structures and reducing defect density are greatly desired for achieving highly sensitive and reliable UV-APDs. As will be discussed in detail, the homoepitaxial growth of AlGaN layers on low dislocation density *n*-type GaN "free-standing" (FS) substrates is a practical and viable means to reduce the leakage current and boost gains significantly (e.g., compared to similar devices grown on non-native GaN/sapphire substrates) through minimizing the density of dislocations propagating from the substrate [18-20].

To improve collection efficiency and sensitivity from weak light, arrays of UV-APDs having large detection sizes are advantageous [21,22]. The development of large detection area UV-APD arrays based on III-N materials, however, has likewise been hampered by high dislocation densities originating from heteroepitaxy, in this case primarily those involving structural and passivating layers defects and irregularities, resulting in nonuniformity in the electrical properties of devices and consequently low yields [16]. Moreover, these issues become more critical as the detection areas of the photodiodes are made larger [23]. Therefore, optimizing the fabrication processes, in particular etching and passivation techniques, to reduce sidewall leakage currents is instrumental towards realizing high performance UV-APD arrays and yielding larger detector sizes [24]. We will likewise cover recent development of large-area 4×4 GaN *p-i-n* UV-APD arrays with strain management that encompass these features and technologies for enhanced performance.

In this paper, we discuss the growth, fabrication, and characterization of GaN and AlGaN *p-i-n* UV-APDs and 4×4 UV-APD arrays on FS-GaN substrates to address the technological issues associated with crystalline defects and crack formation in AlGaN

APDs [14,17]. In addition, the characteristics of the $Al_{0.05}Ga_{0.95}N$ UV-APDs grown on FS-GaN are compared to those fabricated on sapphire substrates having different threading dislocation densities to better understand the influence of leakage current on the performance and longevity of the devices. The development of GaN and AlGaN *p-i-n* UV-APDs and APD arrays on FS-GaN substrates with low dislocation densities thus addresses the technological issues associated with crystalline defects and crack formation in UV-APDs that have been traditionally been detrimental to device performance and reliability.

2. GROWTH AND FABRICATION OF UV-APDS

Epitaxial growth of front-illuminated GaN/AlGaN *p-i-n* UV-APD arrays was carried out by metalorganic chemical vapor deposition (MOCVD) using a reactor system equipped with a close-coupled showerhead growth chamber [19]. The upgraded AIXTRON MOCVD growth reactor, shown in Figure 2, provides better uniformity control for material growth of high quality GaN and AlGaN material with doping for GaN/AlGaN UV-APD applications [25]. Trimethylaluminum (TMAl, $Al(CH_3)_3$), trimethylgallium (TMGa, $Ga(CH_3)_3$), and ammonia (NH_3) were used as the Group III and Group V precursors for aluminum (Al), gallium (Ga), and nitrogen (N), respectively, with hydrogen (H_2) carrier gas for the growth of the $Al_xGa_{1-x}N$ layers. Diluted silane (SiH_4) and bis-cyclopentadienyl magnesium (Cp_2Mg, $Mg(C_5H_5)_2$) were used as *n*-type and *p*-type dopant precursors, respectively.
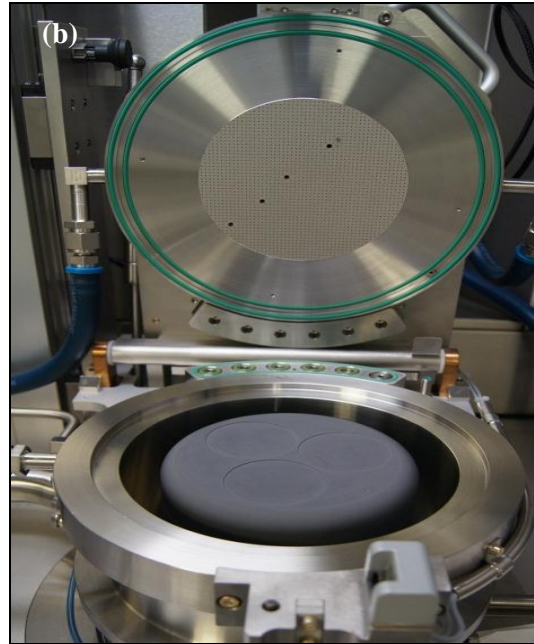
Figure 2. (a) High-temperature MOCVD system (AIXTRON) with close-coupled showerhead used in this work; and (b) III-nitride MOCVD growth chamber, open for loading wafers [25].

The native *n*-type FS-GaN substrates employed, characterized by threading dislocation densities lower than 5×10^6 cm^{-2}, were sliced from a thick GaN layer grown by hydride vapor phase epitaxy. (In prior experiments, double-side polished AlN substrates were utilized in the fabrication of backside-illuminated UV-APD devices [1,26]. A main advantage of GaN-based substrates is maturity of the substrate technology that facilitates implementation of III-N epitaxial growth [27].) For the AlGaN APDs developed on sapphire, GaN/sapphire templates grown on (0001) *c*-plane Al_2O_3 substrates were used; these incorporated a low temperature GaN buffer layer, followed by a ~3 μm thick unintentionally doped GaN layer via two-step growth. The dislocation density of the GaN/sapphire templates was estimated to be ~5.4×10^8 cm^{-2}, based on full-width at half maximum (FWHM) values in X-ray diffraction (XRD) rocking curves. The determined $Al_x Ga_{1-x}N$ mole fraction of $x = 0.05$ was likewise derived from XRD analysis.

The epitaxial layer structure was fabricated into top-illuminated UV-APD individual and array devices with circular mesas of various diameters ranging from 30 μm to 100 μm. (For the 4×4 GaN UV-APD device arrays, each element in the array was patterned into a 75×75 μm^2 square mesa.) Fabrication of the *p-i-n* GaN/$Al_{0.05}Ga_{0.95}N$ UV-APDs was initiated with mesa formation employing inductively coupled plasma (ICP) etching using a Cl_2/Ar carrier gas mixture and silicon dioxide (SiO_2) etch. After

mesa formation, Ti/Al/Ti/Au and Ni/Ag/Ni/Au metal stacks were deposited by electron-beam evaporation and annealed at 700°C and 500°C for the *n*-type and *p*-type ohmic contact layers, respectively. Figure 3(a) shows an epitaxial cross-sectional view of a 30 μm diameter GaN UV-APD device, with a top-view scanning electron microscopy (SEM) image of the device given in Figure 3(b) [27].
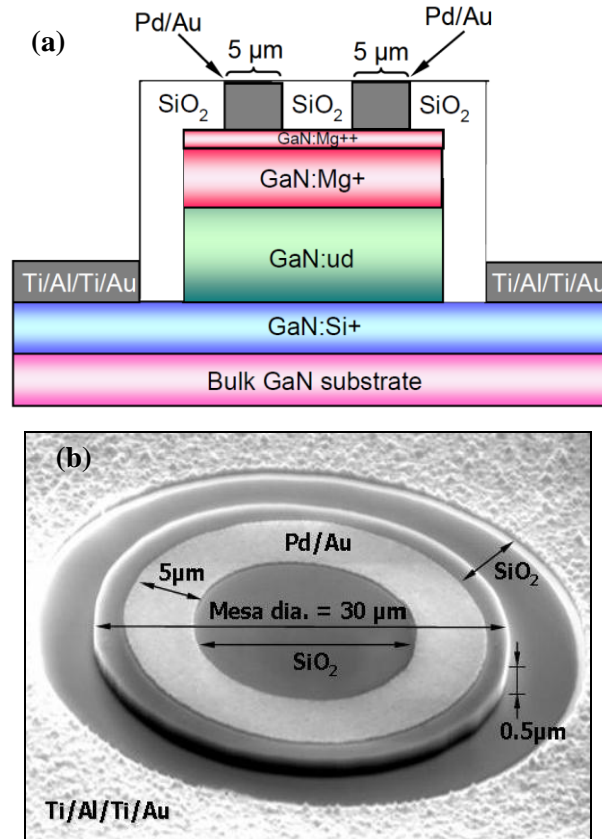

Figure 3. (a) Schematic structure, and (b) corresponding scanning electron microscopy (SEM) image, of 30 μm diameter GaN APD with 5 μm wide Pd/Au ring, fabricated in this instance without bonding pads [27].

The fabricated devices were then passivated by SiO_2 using plasma-enhanced chemical vapor deposition (PECVD). The passivation layer was designed to reduce the leakage current through the mesa sidewalls, preventing the devices from undergoing premature breakdown under reverse bias. A portion of this SiO_2 layer was subsequently removed by ICP etching to form via holes for interconnects and wire bonding pads. Finally, thick Ti/Au metal stacks forming the metal interconnects and

bonding pads were deposited by electron-beam evaporation. Figure 4(a) shows a schematic cross-sectional view of the epitaxial layers and device structure for the $Al_{0.05}Ga_{0.95}N$ UV-APDs, and Figure 4(b) features a top-view SEM image of the APD physical layout showing the metal contact pads and circular mesa, where the dotted yellow line (*A* to *A'*) indicates the extent of the cross-sectional portion depicted schematically in Figure 4(a) [17].
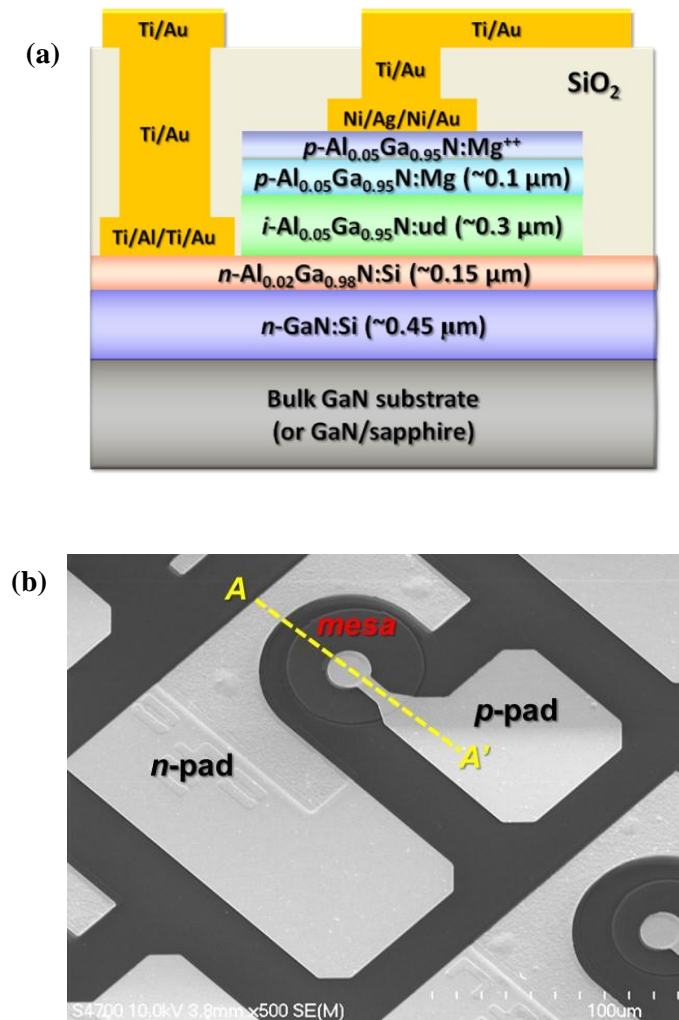

Figure 4. (a) Device structure cross-section of GaN *p-i-n* APD on bulk GaN substrate. (b) Corresponding SEM image showing contact pads and circular mesa area of photodiode [17].
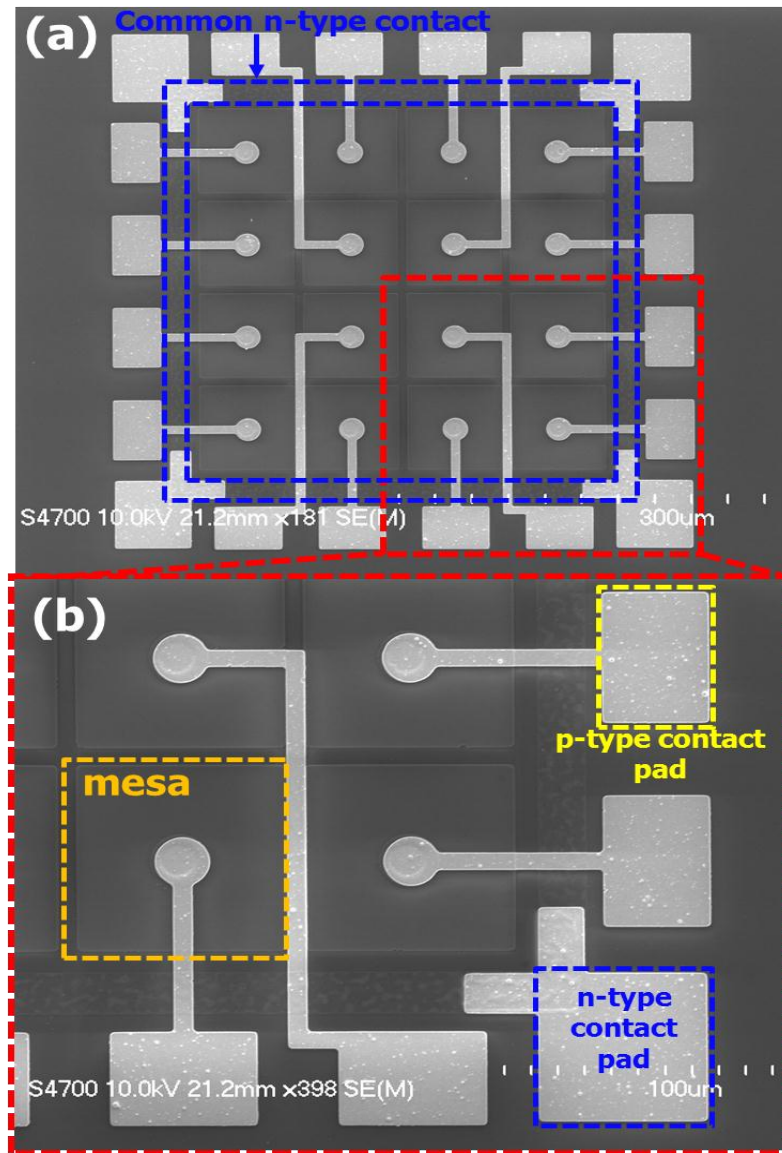
Figure 5. Top-view SEM image of (a) 4×4 GaN *p-i-n* UV-APD array with 75×75 µm² mesas grown on FS-GaN substrate; and (b) expanded portion of UV-APD array in lower-right quadrant of image in (a) [14].

A top-view SEM image of the fabricated front-illuminated GaN *p-i-n* UV-APD array is shown in Figure 5, comprising 16 individual GaN UV-APDs spaced 7 µm apart from one another [14]. Four square wire *n*-type bonding pads are present at each corner, connected to a common *n*-type contact situated around the periphery of the UV-APD array. Along every side of the UV-APD array are the rectangular wire-bonding pads for the *p*-type contacts, one for each of the 16 devices.

XRD rocking curves were used to characterize the bulk crystalline quality of the epitaxial layer structures of the UV-APDs. XRD ω-2θ scans near a GaN (00·4) diffraction peak are shown in Figure 6 [24]. Although the $Al_{0.05}Ga_{0.95}N$ *p-i-n* UV-APD on FS-GaN substrate (black line) and that on the GaN/sapphire template (red line) were fabricated with the same growth conditions, it is seen that the XRD peaks corresponding to the individual layers in their epitaxial structures differ marginally. This may be attributed to the variation in actual substrate surface temperatures caused by different substrate thermal conductivities, and likewise to the strain/bowing status of the growing surfaces that is known to vary according to substrate type [25].
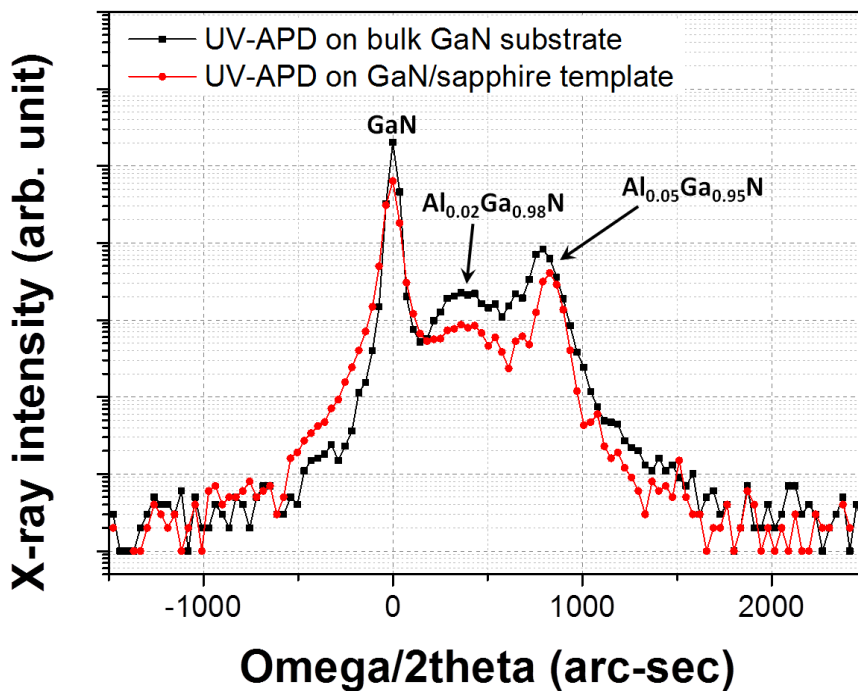

Figure 6. X-ray diffraction (XRD) ω-2θ scans near GaN diffraction condition for $Al_{0.05}Ga_{0.95}N$ *p-i-n* UV-APDs grown on FS-GaN substrate (black line) and GaN/sapphire template (red line) [24].

In addition, atomic-force microscopy (AFM) was utilized to characterize the surface properties of the UV-APD arrays. Figure 7 shows plots of the root mean square (RMS) surface roughness of the structures with various AFM scan sizes [24]. The AlGaN UV-APD epitaxial structures grown both on FS-GaN and GaN/sapphire substrates had well-developed atomic step-flow morphologies, and no defects were observed on the surfaces from the AFM analysis. However, the epitaxial layers grown on the GaN/sapphire template evidenced dislocation-related surface features not observed in those grown on the FS-GaN substrate. These results support the

practicality of developing low-cost, highly uniform, and reproducible UV-APD arrays on bulk GaN substrates.

Figure 8 presents chemical analysis of major dopants and potential impurities in the epitaxial structure performed using secondary ion mass spectrometry (SIMS) of the GaN *p-i-n* APD structure [28]. The Si and Mg dopant profiles confirm that the epitaxial structure matches well with the APD design. The impurity levels for C and O remain close to the detection limit of the SIMS instrument.
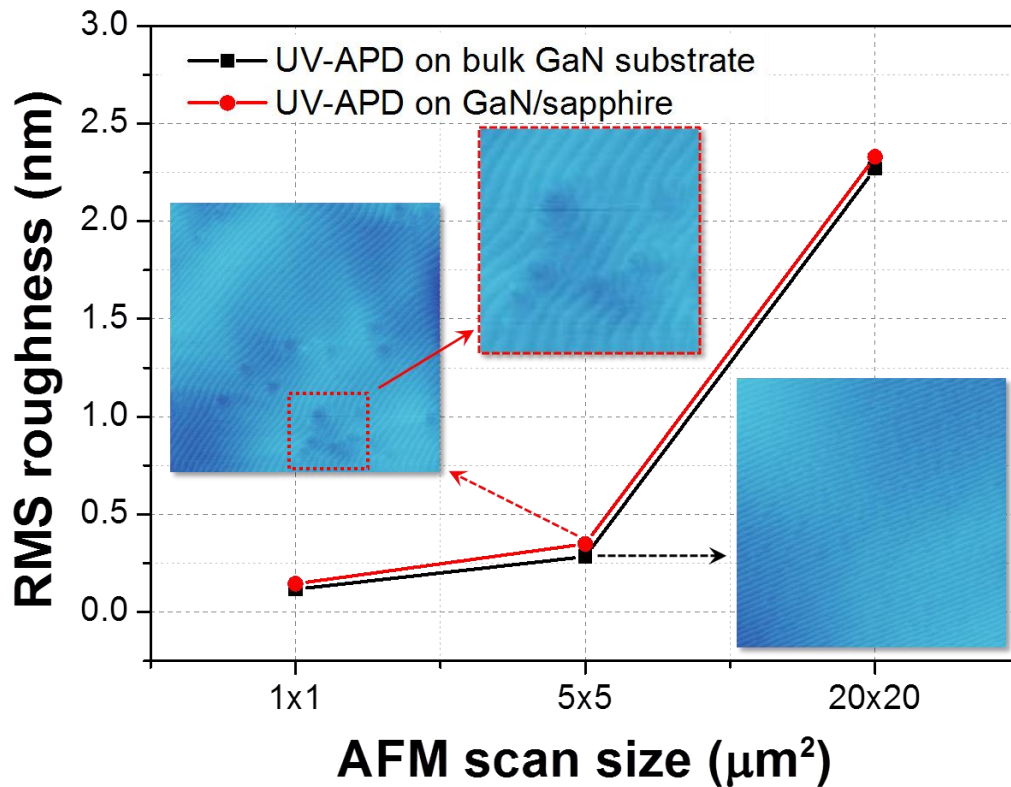

Figure 7. Atomic force microscopy (AFM) RMS roughness of $Al_{0.05}Ga_{0.95}N$ *p-i-n* UV-APDs grown on a FS-GaN substrate (black squares) and a GaN/sapphire template (red circles) with different scan areas; *inset* shows surface images in 5×5 μm^2 scan [24].
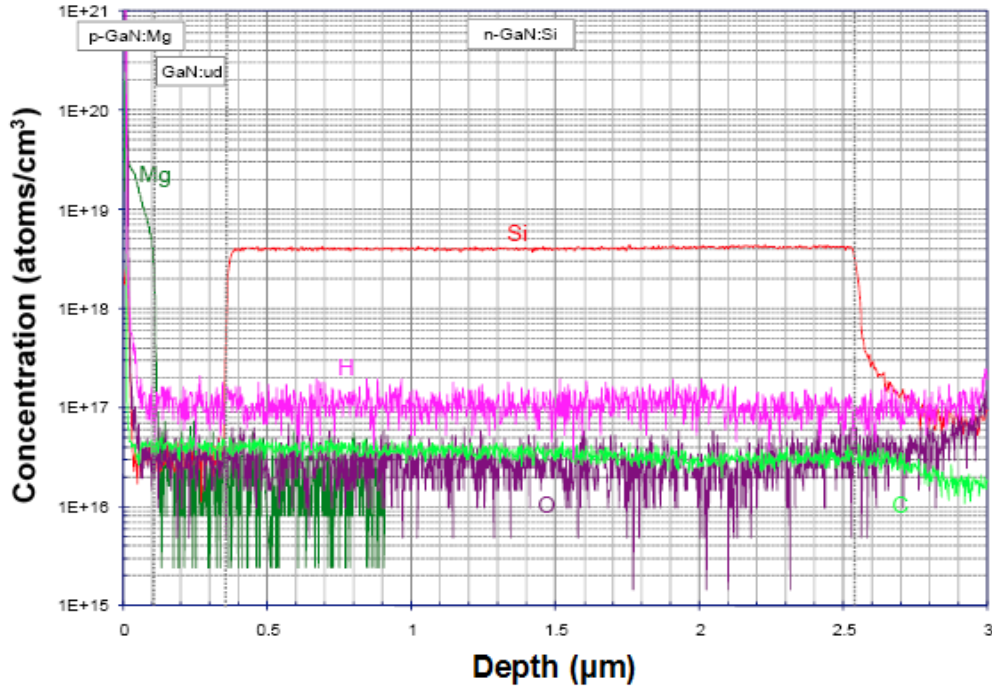
Figure 8. Secondary ion mass spectrometry (SIMS) profile of GaN *p-i-n* APD structure. The data show controlled Si and Mg doping for *n-* and *p*-type layers, respectively, and low background doping concentration in the *i*-GaN layer [28].

3. UV-APD DEVICE PERFORMANCE RESULTS

In order to measure the dark current, photocurrent, and avalanche gain of the GaN/AlGaN UV-APD devices, a Keithley Model 4200 semiconductor characterization system and Newport Apex illuminator with Oriel xenon lamp equipped with a monochromator system were utilized. The avalanche gain was calculated as the difference between the reverse-biased photocurrent and the dark current, divided by the difference between the low-bias photocurrent and the dark current. To obtain the photocurrent distributions, UV light at the 280 nm solar-blind wavelength was used to illuminate the front surfaces of the UV-APDs.

Figure 9 shows the dark current, photocurrent, and avalanche gain for a $Al_{0.05}Ga_{0.95}N$ UV-APD with 30 μm diameter circular mesa as a function of reverse bias. Under dark conditions, the device showed low leakage current under 1 pA (corresponding to dark current density of less than 1×10^{-7} A/cm^2) up to a reverse voltage of around 60 V [17]. Above 60 V, however, the dark current increased monotonically until the impact ionization process started to dominate the current flow, indicating increased generation current from the bulk space-charge region with increasing reverse bias [20]. Beyond this point, the dark current rose sharply with increasing reverse bias,

suggesting active impact ionization in the multiplication region. Under the 280 nm UV illumination, the photocurrent remained constant up to 60 V, and then for higher values of reverse bias rose noticeably over the dark current background (see Figure 9, *inset*). At the onset of avalanche breakdown (102 V), the avalanche gain for this device reached a maximum value of above 2×10^6, indicating strong avalanche multiplication processes. In addition, no microplasma breakdown or edge breakdown due to sidewall damage were determined to occur, the absence of which is attributed to the low damage etching process and high quality dielectric passivation utilized for the UV-APD.
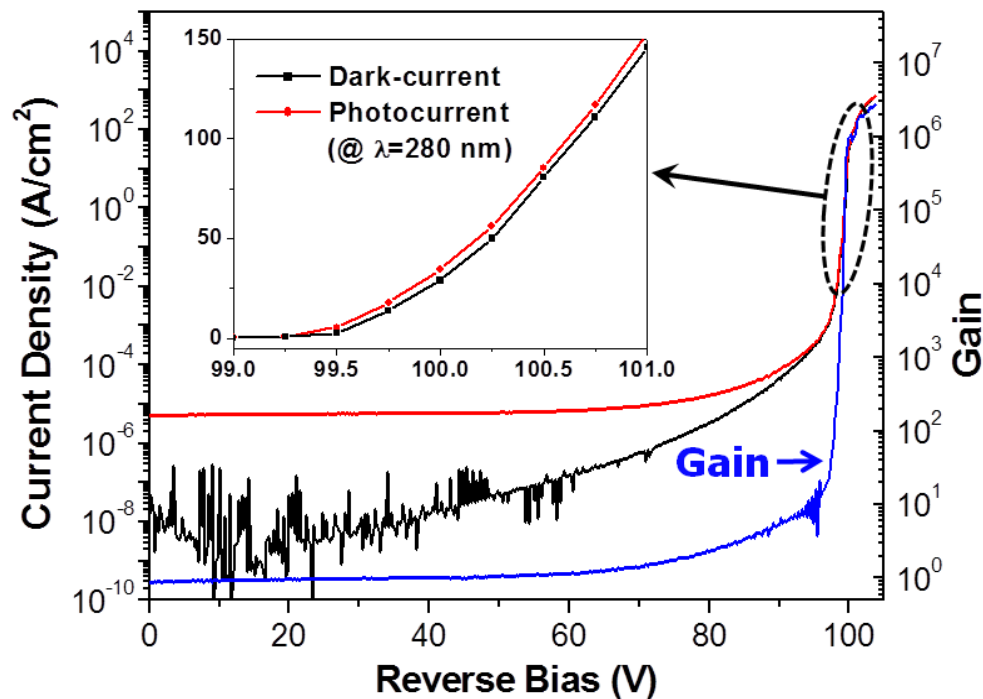

Figure 9. Current density and gain plotted vs. reverse bias for an Al$_{0.05}$Ga$_{0.95}$N UV-APD with mesa diameter of 30 μm with and without UV illumination at 280 nm. *Inset* shows dark current and photocurrent plotted over 99 V to 101 V reverse bias range [17].

Figure 10 presents a comparison of the reverse bias *I-V* characteristics of 40 μm diameter Al$_{0.05}$Ga$_{0.95}$N UV-APDs grown on a FS-GaN substrate and GaN/sapphire template [24]. For the UV-APD device grown on the FS-GaN substrate [Figure 10(a)], the dark current is shown to increase sharply above the onset point of avalanche breakdown (~100 V). The maximum electric field of the device was estimated to be ~3.2 MV/cm, consistent with values reported in literature for

avalanche breakdown multiplication. The estimated avalanche gain was 82 at the onset point and became higher than 5×10^5 beyond the breakdown voltage (V_{BR}) of 102 V. This sharp increment of avalanche gain implies that the device underwent a strong avalanche multiplication process above V_{BR}.
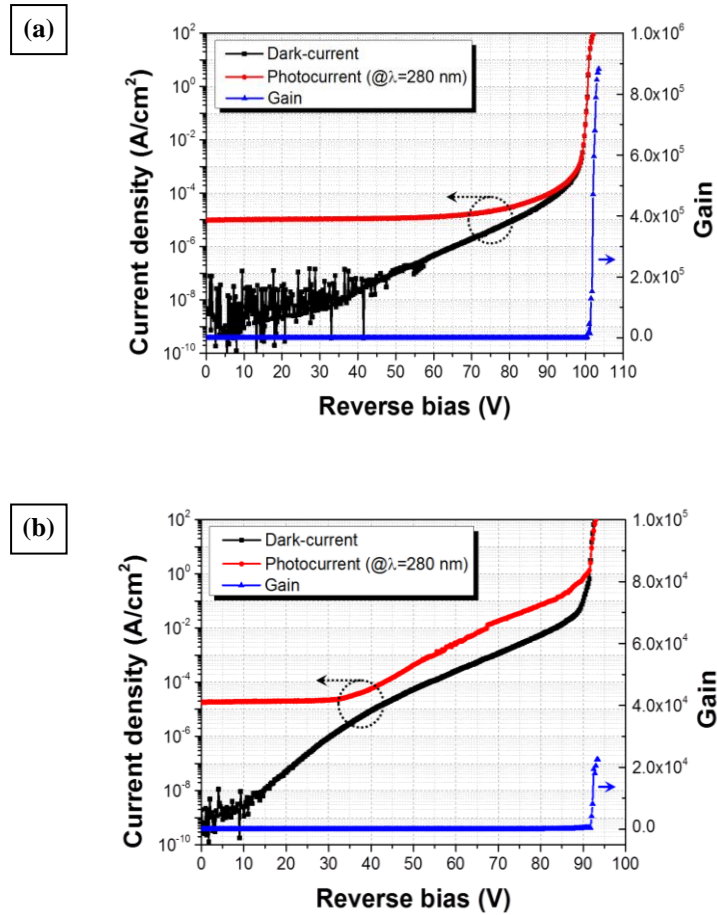

Figure 10. Reverse-based *I-V* characteristics for 40 μm diameter Al$_{0.05}$Ga$_{0.95}$N *p-i-n* UV-APDs grown on (a) FS-GaN substrate and (b) GaN/sapphire template [24].

Figure 10(b) plots the gain and dark current density for the corresponding Al$_{0.05}$Ga$_{0.95}$N UV-APD device grown on the GaN/sapphire template. The averaged dark current densities taken up to the onset point were ~3.1×10^{-6} A/cm^2 for AlGaN UV-APDs grown on the FS-GaN substrate, and ~6.5×10^{-5} A/cm^2 for those grown on the GaN/sapphire template; in the case of the latter, the dark current density increased dramatically even at low reverse bias. The comparatively high dark current of the

UV-APD grown on the GaN/sapphire template was determined to be the result of higher dislocation density in its active region, resulting in detrimental trap-assisted leakage current. The calculated avalanche gain of the UV-APD grown on the GaN/sapphire template became higher than 2×10^4 at the V_{BR} of ~93 V. Though avalanche breakdown was observed, the avalanche gain of the UV-APD grown on the GaN/sapphire template was still an order of magnitude lower than the gain of the UV-APD grown on the FS-GaN substrate [Figure 10(a)].

Figure 11(a) presents the breakdown voltages and dark current densities of $Al_{0.05}Ga_{0.95}N$ UV-APDs with those of GaN UV-APDs having similar *p-i-n* epitaxial layer structures, all grown on FS-GaN substrates, as functions of APD mesa area [17]. The breakdown voltages of the UV-APD devices of various mesa sizes were in the range of 94 V to 102 V. The relatively small but significant differences in V_{BR} between the $Al_{0.05}Ga_{0.95}N$ and GaN UV-APDs may be attributed in part to the devices having slightly different drift region thicknesses. The averaged dark current densities for the AlGaN devices increased overall with mesa area, while these values remain less than 5×10^{-7} A/cm^2 for all mesa area devices; this was likewise the case for the GaN UV-APDs [11].

Figure 11(b) plots the photocurrent densities at a wavelength of 280 nm taken from the flat region of the *I-V* plots under 60 V reverse bias along with the maximum avalanche gains of the $Al_{0.05}Ga_{0.95}N$ UV-APDs, again as functions of mesa area [17]. The unity-gain photocurrent density showed relatively uniform distribution for each measured device, though some dependence on mesa size is evident. The avalanche gain for all the devices remained greater than 1.5×10^5, which is significantly higher than that previously reported for $Al_{0.05}Ga_{0.95}N$ UV-APDs [29]. The low leakage current preceding avalanche breakdown, consistent breakdown behavior, and high avalanche gain for the $Al_{0.05}Ga_{0.95}N$ UV-APDs are attributed to the improved crystalline quality of the optimized epitaxial layers and reduced defect densities effected through strain management in the *n*-$Al_xGa_{1-x}N$ step graded layers.
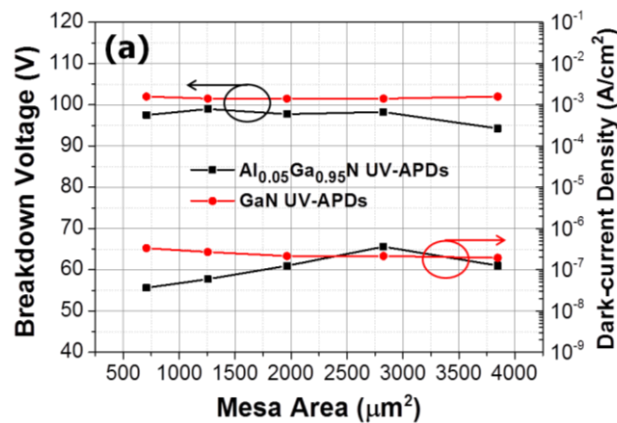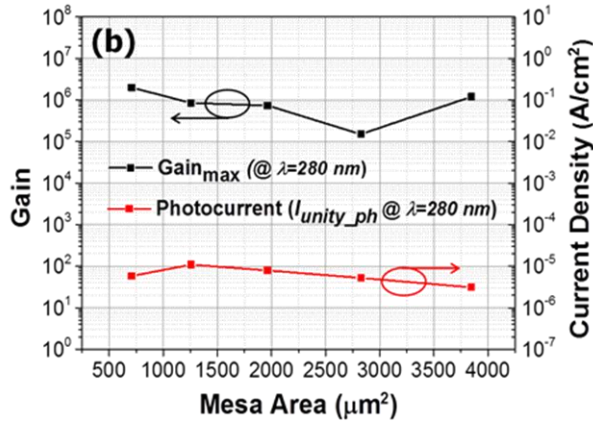
Figure 11. Area-dependent breakdown voltages and dark current densities of $Al_{0.05}Ga_{0.95}N$ UV-APDs compared with those of GaN UV-APDs, both grown on FS-GaN substrates, and (b) photocurrent densities and avalanche gains of the $Al_{0.05}Ga_{0.95}N$ UV-APDs under 280 nm UV illumination [17].

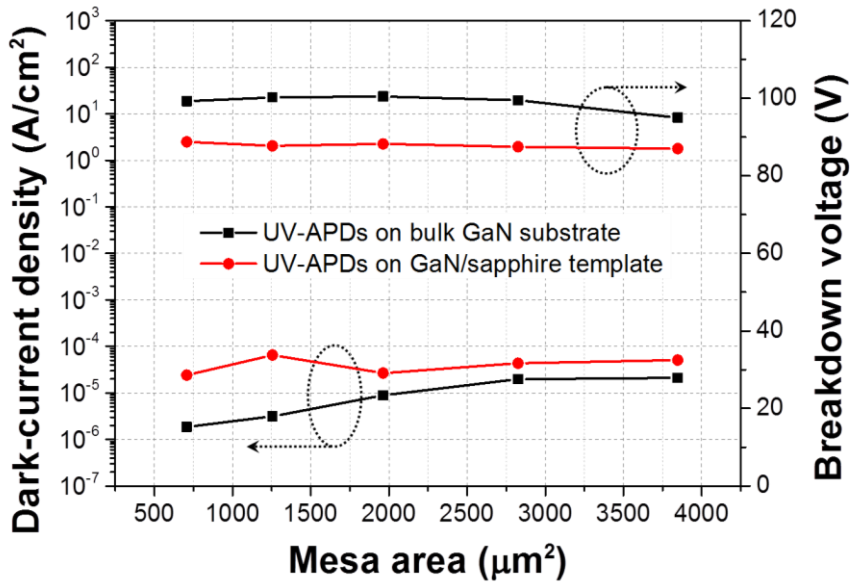**Figure 12.** Area-dependent dark current densities and breakdown voltages of $Al_{0.05}Ga_{0.95}N$ UV-APDs grown on a FS-GaN substrate and a GaN/sapphire template [24].

Figure 12 shows the dependence of the dark current densities and breakdown voltages on APD mesa area for $Al_{0.05}Ga_{0.95}N$ *p-i-n* UV-APDs grown on FS-GaN substrates as well as GaN/sapphire templates [24]. These devices were characterized by mesas

ranging from 30 μm to 70 μm in diameter, corresponding to surface areas of 707 μm^2 to 3847 μm^2, respectively. Concerning the smaller devices (areas less than 1500 μm^2), the dark current densities were approximately one order of magnitude lower for APDs on the FS-GaN substrates than those on the GaN/sapphire templates, while for larger devices (areas greater than 2500 μm^2) they differed only by a factor of 2 to 3. The small changes in dark current density with respect to mesa sizes in Figure 12 potentially indicate minimal damage occurring in the mesa definition, with the high quality dielectric passivation contributing towards reducing leakage current through the mesa sidewall surfaces.
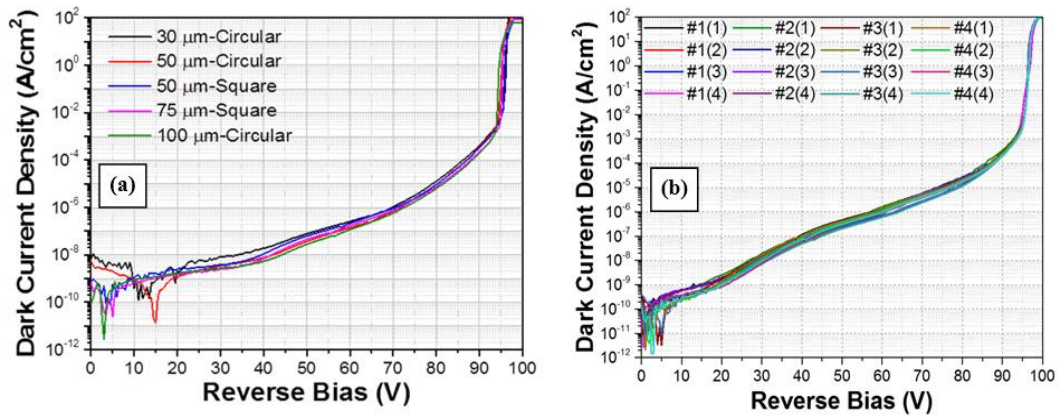

Figure 13. (a) Dark currents for independent UV-APDs with various mesa sizes and shapes; and (b) repetitive reverse bias *I-V* characteristics of four different devices selected from 4×4 GaN UV-APD array grown on a FS-GaN substrate [14].

Figure 13(a) displays the correlation with mesa area of the reverse bias *I-V* characteristics of individual UV-APDs similar to and representing those in the 4×4 GaN UV-APD arrays grown on FS-GaN [14]. It is seen that the dark currents of the single UV-APDs rose until impact ionization effects started to affect the current flow at around 94 V reverse bias, marking the onset of avalanche breakdown. Beyond this voltage, the dark current density rose sharply with increasing reverse bias, suggesting the occurrence of active impact ionization under the high electric field in the multiplication region. These devices fabricated with different mesa sizes exhibited almost identical reverse bias characteristics in terms of dark/leakage current and V_{BR}.

Additionally, multiple reverse bias *I-V* scans of dark current behavior were performed for selected devices along the diagonal of the 4×4 *p-i-n* UV-APD arrays to verify the reliability of the devices, with these results plotted in Figure 13(b). Similar to the

pattern seen in Figure 13(a), the four UV-APD devices chosen exhibited nearly identical dark currents and consistent breakdown voltages over repetition of the *I-V* scans [14]. The average dark current leading up to the onset point of breakdown voltage (approximately 96 V for all the UV-APD devices) was determined to be $\sim 2.6 \times 10^{-7}$ A/cm^2. These concurrent *I-V* characteristics measured over the sequential tests demonstrated consistent breakdown voltage and leakage current behavior. The stable and reliable electrical properties of the measured UV-APDs are attributed in part to suppressed mesa sidewall leakage currents and local junction breakdown.

The reverse bias dependent spectral response of both the GaN and Al$_{0.05}$Ga$_{0.95}$N *p-i-n* UV-APD devices was likewise characterized at room temperature.   For this measurement setup involving frontside illumination, an Oriel xenon lamp, Cornerstone 260 monochromator/chopper system, and lock-in amplifier were utilized for the UV radiation source, selection and modulation of the optical wavelength, and photocurrent measurement, respectively. Figure 14 shows the bias-dependent spectral responsivity vs. wavelength under varied reverse biases of selected Al$_{0.05}$Ga$_{0.95}$N GaN and UV-APD devices grown on FS-GaN substrates. In contrast to UV-APDs grown on the GaN/sapphire templates, premature microplasma breakdown resulting from defects and dislocations in the active regions was not observed for the Al$_{0.05}$Ga$_{0.95}$N UV-APDs grown on FS-GaN substrates.
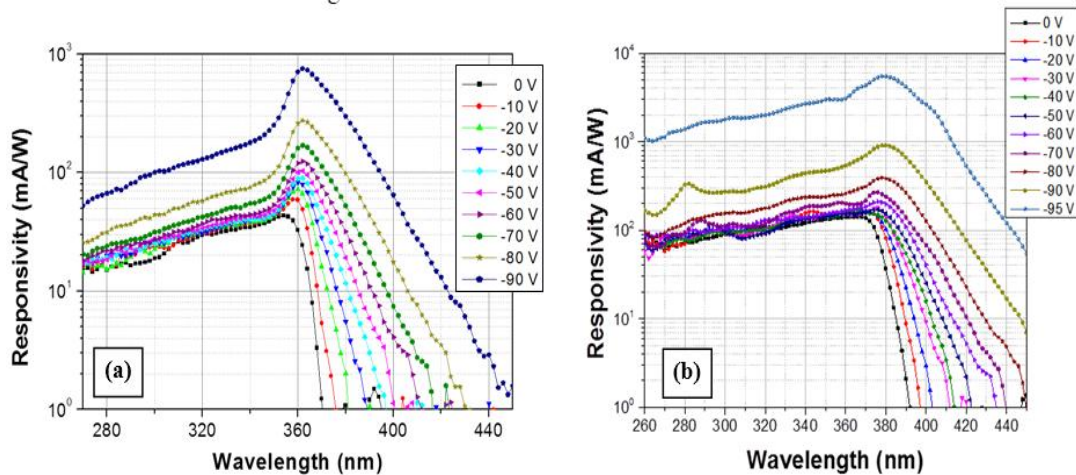
Figure 14. (a) Reverse-biased voltage-dependent spectral response of photocurrent measured at room temperature for 70 μm diameter Al$_{0.05}$Ga$_{0.95}$N *p-i-n* UV-APD [24]. (b) Reverse bias dependent spectral response of a selected device from GaN *p-i-n* UV-APD array with mesa size of 75×75 μm^2 [14].

In Figure 14(a), a 70 μm diameter Al$_{0.05}$Ga$_{0.95}$N UV-APD showed peak responsivity of 43.4 mA/W at 354 nm under zero bias, corresponding to an external quantum

efficiency (EQE) of ~16% [24]. However, at a reverse bias of 80 V closer to the breakdown voltage, the peak responsivity increased to 221.8 mA/W at 362 nm, corresponding to an EQE ~94%. (The occurrence of significant UV absorption in the p-Al$_{0.05}$Ga$_{0.95}$N layer of the frontside-illuminated UV-APD device is noted, somewhat limiting the attainable EQE.) The peak absorption wavelength for the photocurrent at zero bias (measured at ~354 nm) was found to correspond to the bandgap of the Al$_{0.05}$Ga$_{0.95}$N layer. In addition, this AlGaN device exhibited a zero-bias absorption cutoff wavelength of 370 nm, about 10 nm shorter than that of GaN *p-i-n* APDs.

The responsivity curves vs. wavelength for a 75×75 μm^2 GaN *p-i-n* device selected from a 4×4 UV-APD array are given in Figure 14(b) [14]. For this device, a peak responsivity of 142 mA/W at zero bias was exhibited at a wavelength of 366 nm with an absorption edge at 390 nm. The peak absorption wavelength was observed to shift from 366 nm to 378 nm with increasing reverse bias, which is possibly related to the Franz-Keldysh effect [19]. Concerning both the GaN and Al$_{0.05}$Ga$_{0.95}$N UV-APDs, the significantly broadened absorption edges moving into the bluer (shorter-wavelength) bands at larger reverse biases indicates the extension of the depletion region into the *p-* and *n*-type doped regions as the electric field increased. Likewise, the significant rise in the responsivities at comparatively high values of reverse bias (particularly 90 V and above) was determined to be the result of carrier impact ionization approaching the onset of avalanche multiplication.

4. SUMMARY AND CONCLUSIONS

This paper has examined the growth and characterization of GaN and Al$_{0.05}$Ga$_{0.95}$N epitaxial device structures that have demonstrated low dark current densities and high gains at avalanche breakdown. GaN/AlGaN *p-i-n* UV-APDs grown by MOCVD on a free-standing GaN substrates exhibited avalanche gains greater than 2×10^5 and zero-bias responsivities above 140 mA/W (with considerably higher values measured near the onset of avalanche breakdown). Optimized growth and doping parameters of the epitaxial *p-i-n* structures and a sophisticated UV-APD array fabrication process were applied to minimize both bulk and surface leakage currents.

While premature microplasma breakdown was frequently observed for UV-APDs grown on GaN/sapphire templates, the GaN and Al$_{0.05}$Ga$_{0.95}$N UV-APDs grown on the FS-GaN substrates demonstrated lower dark current densities and more consistent avalanche breakdown. In addition, the avalanche gains of the Al$_{0.05}$Ga$_{0.95}$N UV-APDs grown on FS-GaN were over an order of magnitude higher than those for comparable UV-APDs on GaN/sapphire.

Likewise, the GaN 4×4 UV-APD arrays showed relatively uniform and stable leakage current distribution among UV-APDs, with dark/leakage current densities below ~6.5×10^{-7} A/cm^2. The significantly improved photoresponse observed for these

devices at reverse biases greater than 90 V is indicative of the contributions of a strong avalanche multiplication process. Furthermore, repeated reverse-bias *I-V* scans showed no meaningful difference in the measured dark currents and breakdown voltages, establishing consistent and reliable UV-APD device performance.

In summary, high quality MOCVD epitaxial growth and associated low dislocation densities in the active layers of AlGaN UV-APDs grown on native free-standing GaN substrates have enabled suppressed microplasma breakdown and low dark current densities, resulting in comparatively high photocurrents and responsivities at solar-blind wavelengths. The consequent improvements in GaN/AlGaN APD performance and reliability are key towards the development and successful implementation of robust, highly sensitive, larger format UV-APD focal plane arrays expected to play a vital role in future advanced defense and commercial systems to address an array of high resolution UV imaging applications.

REFERENCES

[1]   A. K. Sood, J. W. Zeller, R. E. Welser, Y. R. Puri, M.-H. Ji, J. Kim, T. Detchprohm, R. D. Dupuis, N. K. Dhar, and P. Wijewarnasuriya, "Development of high gain avalanche photodiodes for UV imaging applications," *Proc. SPIE* **9609**, 96090X (2015).

[2]   A. K. Sood, J. W. Zeller, R. E. Welser, Y. R. Puri, R. D. Dupuis, M.-H. Ji, J. Kim, T. Detchprohm, J. Lewis, and N. K. Dhar, "Development of GaN/AlGaN UVAPDs for ultraviolet sensor applications," *Int. J. Phys. Appl.* **7**(1), 49-58 (2015).

[3]   J. P. Long, "UV detectors and focal plane array imagers based on AlGaN *p-i-n* photodiodes," *Opto-Electron. Rev.* **10**(4), 251-260 (2002).

[4]   M. B. Reine, A. Hairston, P. Lamarre, K. K. Wong, S. P. Tobin, A. K. Sood, C. Cooke, M. Pophristic, S. Guo, B. Peres, R. Singh, C. R. Eddy, Jr., U. Chowdhury, M. M. Wong, R. D. Dupuis, T. Li, and S. P. DenBaars, "Solar blind AlGaN 256x256 pin detectors and focal plane arrays," *Proc. SPIE* **6121**, 61210R (2006).

[5]   N. K. Dhar, "IR Material Research at the Army Research Laboratory," *Proc. SPIE* **6542**, 65420C (2007).

[6]   A. K. Sood, R. A. Richwine, Y. R. Puri, N. K. Dhar, D. L. Polla, and P. S. Wijewarnasuriya, "Multispectral EO/IR sensor model for evaluating UV, visible, SWIR, MWIR and LWIR system performance," *Proc. SPIE* **7300**, 73000H (2009).

[7]   S. Choi, H. J. Kim, Y. Zhang, X. Bai, D. Yoo, J. Limb, J.-H. Ryou, S.-C. Shen, P. D. Yoder, and R. D. Dupuis, "Geiger-mode operation of GaN avalanche

photodiodes grown on GaN substrates," *IEEE Photon. Tech. Lett.* **21**(20), 1526-1528 (2009).

[8] Z. G. Shao, D. J. Chen, H. Lu, R. Zhang, W. J. Luo, Y. D. Zheng, L. Li, and Z. H. Li, "High-gain AlGaN solar-blind avalanche photodiodes," *IEEE Electron. Dev. Lett.* **35**(3), 372-374 (2014).

[9] J. Qu, J. Li, and G. Zhang, "AlGaN/GaN heterostructure grown by metalorganic vapor phase epitaxy," *Solid State Comm.* **107**(9), 467-470 (1998).

[10] J. L. Pau, C. Bayram, R. McClintock, M. Razeghi, and D. Silversmith, "Back-illuminated separate absorption and multiplication GaN avalanche photodiodes," *Appl. Phys. Lett.* **92**(10), 101120 (2008).

[11] X. Wang, W. Hu, M. Pan, L. Hou, W. Xie, J. Xu, X. Li, X. Chen, and W. Lu, "Study of gain and photoresponse characteristics for back-illuminated separate absorption and multiplication GaN avalanche photodiodes," *J. Appl. Phys.* **115**(1), 013103 (2014).

[12] Y. Huang, D. J. Chen, H. Li, K. X. Dong, R. Zhang, Y. D. Zheng, L. Li, and Z. H. Li, "Back-illuminated separate absorption and multiplication AlGaN solar-blind avalanche photodiodes," *Appl. Phys. Lett.* **101**(25), 253516 (2012).

[13] Z. Huang, J. Li, W. Zhang, and H. Jiang, "AlGaN solar-blind avalanche photodiodes with enhanced multiplication gain using back-illuminated structure," *Appl. Phys. Expr.* **6**(5), 054101 (2013).

[14] M.-H. Ji, J. Kim, T. Detchprohm, R. D. Dupuis, A. K. Sood, N. K. Dhar, and J. Lewis, "Uniform and reliable GaN *pin* ultraviolet avalanche photodiode arrays." *IEEE Photon. Tech. Lett.* **28**(19), 2015-2018 (2016).

[15] Q. Zhou, D. C. McIntosh, Z. Lu, J. C. Campbell, A. V. Sampath, H. Shen, and M. Wraback, "GaN/SiC avalanche photodiodes," *Appl. Phys. Lett.* **99**(13), 131110 (2011).

[16] E. Cicek, Z. Vashaei, R. McClintock, C. Bayram, and M. Razeghi, "Geiger-mode operation of ultraviolet avalanche photodiodes grown on sapphire and free-standing GaN substrates," *Appl. Phys. Lett.* **96**(26), 261107 (2010).

[17] J. Kim, M.-H. Ji, T. Detchprohm, J.-H. Ryou, R. D. Dupuis, A. K. Sood, and N. K. Dhar, "Al$_x$Ga$_{1-x}$N ultraviolet avalanche photodiodes with avalanche gain greater than 10^5," *IEEE Photon. Tech. Lett.* **27**(6), 642-645 (2015).

[18] J. B. Limb, D. Yoo, J.-H. Ryou, W. Lee, S. C. Shen, R. D. Dupuis, M. L. Reed, C. J. Collins, M. Wraback, D. Hanser, E. Preble, N. M. Williams, and K. Evans, "GaN ultraviolet avalanche photodiodes with optical gain greater than 1000 grown on GaN substrates by metal-organic chemical vapor deposition," *Appl. Phys. Lett.* **89**(1), 011112 (2006).

[19] S.-C. Shen, Y. Zhang, D. Yoo, J. B. Limb, J.-H. Ryou, P. D. Yoder, and R. D.

Dupuis, "Performance of deep ultraviolet GaN avalanche photodiodes grown by MOCVD," *IEEE Photon. Tech. Lett.* **19**(21), 1744-1746 (2007).

[20] Y. Zhang, S.-C. Shen, H. J. Kim, S. Choi, J.-H. Ryou, R. D. Dupuis, and B. Narayan, "Low-noise GaN ultraviolet *p-i-n* photodiodes on GaN substrates," *Appl. Phys. Lett.* **94**(22), 221109 (2009).

[21] W. B. Liu, D. G. Zhao, X. Sun, S. Zhang, D. S. Jiang, H. Wang, S. M. Zhang, Z. S. Liu, J. J. Zhu, Y. T. Wang, and L. H. Duan, "Stable multiplication gain in GaN *p-i-n* avalanche photodiodes with large device area," *J. Phys. D: Appl. Phys* **42**(1), 015108 (2009).

[22] F. Yan, C. Qin, J. H. Zhao, M. Bush, G. Olsen, B. K. Ng, J. P. R. David, R. C. Tozer, and M. Weiner, "Demonstration of 4H-SiC avalanche photodiodes linear array," *Solid-State Electron.* **47**(2), 241-245 (2003).

[23] K. Minder, J. L. Pau, R. McClintock, P. Kung, C. Bayram, M. Razeghi, and D. Silversmith, "Scaling in back-illuminated GaN avalanche photodiodes," *Appl. Phys. Lett.* **91**(7), 073513 (2007).

[24] J. Kim, M.-H. Ji, T. Detchprohm, R. D. Dupuis, J.-H. Ryou, A. K. Sood, N. K. Dhar, and J. Lewis, "Comparison of AlGaN *p-i-n* ultraviolet avalanche photodiodes grown on free-standing GaN and sapphire substrates," *Appl. Phys. Expr.* **8**(12), 122202 (2015).

[25] A. K. Sood, R. A. Richwine, R. E. Welser, Y. R. Puri, R. D. Dupuis, M.-H. Ji, J. Kim, T. Detchprohm, N. K. Dhar, and R. L. Peters, "Development of III-N UVAPDs for ultraviolet sensor applications," *Proc. SPIE* **8868**, 88680T (2013).

[26] S. Choi, H. J. Kim, J.-H. Ryou, and R. D. Dupuis, "Actual temperatures of growing surfaces of III-nitride-based materials depending on substrates and forced convection conditions in metal organic chemical vapor deposition," *J. Appl. Phys.* **106**(7), 073512 (2009).

[27] R. D. Dupuis, J.-H. Ryou, D. Yoo, J. B. Limb, Y. Zhang, S.-C. Shen, and D. Yoder, "High-performance GaN and $Al_xGa_{1-x}N$ ultraviolet avalanche photodiodes grown by MOCVD on bulk III-N substrates," *Proc. SPIE* **6739**, 67391B (2007).

[28] A. K. Sood, R. A. Richwine, R. E. Welser, Y. R. Puri, R. D. Dupuis, J.-H. Ryou, N. K. Dhar, P. Suvarna, and F. Shahedipour-Sandvik, "Development of small unit cell avalanche photodiodes for UV imaging applications," *Proc. SPIE* **8375**, 83750R (2012).

[29] D. Yoo, J. Limb, J.-H. Ryou, Y. Zhang, S.-C. Shen, and R. D. Dupuis, "$Al_xGa_{1-x}N$ ultraviolet avalanche photodiodes grown on GaN substrates," *IEEE Photon. Tech. Lett.* **19**(17), 1313-1315 (2007).